Journal of Alloys and Compounds 509 (2011) 6004–6008

Contents lists available at ScienceDirect

Journal of Alloys and Compounds

journal homepage: www.elsevier.com/locate/jallcom

Structural, optical and electrical properties of $CuIn_5S_8$ thin films grown by thermal evaporation method

M. Gannouni*, M. Kanzari

Laboratoire de Photovoltaïque et Matériaux Semi-conducteurs -ENIT BP 37, Le belvédère 1002-Tunis, Tunisie

ARTICLE INFO

Article history:
Received 20 June 2010
Received in revised form 6 February 2011
Accepted 7 February 2011
Available online 12 February 2011

Keywords:
$CuIn_5S_8$
Spinel structure
Annealing
Optical properties
Electrical properties

ABSTRACT

Stoichiometric compound of copper indium sulfur ($CuIn_5S_8$) was synthesized by direct reaction of high purity elemental copper, indium and sulfur in an evacuated quartz tube. The phase structure of the synthesized material revealed the cubic spinel structure. The lattice parameter (a) of single crystals was calculated to be 10.667 Å. Thin films of $CuIn_5S_8$ were deposited onto glass substrates under the pressure of 10^{-6} Torr using thermal evaporation technique. $CuIn_5S_8$ thin films were then thermally annealed in air from 100 to 300 °C for 2 h. The effects of thermal annealing on their physico-chemical properties were investigated using X-ray diffraction (XRD), Energy-dispersive X-ray spectroscopy (EDX), scanning electron microscope (SEM), optical transmission and hot probe method. XRD studies of $CuIn_5S_8$ thin films showed that as-deposited films were amorphous in nature and transformed into polycrystalline spinel structure with strong preferred orientation along the (3 1 1) plane after the annealing at 200 °C. The composition is greatly affected by thermal treatment. From the optical transmission and reflection, an important absorption coefficient exceeds 10^4 cm^{-1} was found. As increasing the annealing temperature, the optical energy band gap decreases from 1.83 eV for the as-deposited films to 1.43 eV for the annealed films at 300 °C. It was found that $CuIn_5S_8$ thin film is an n-type semiconductor at 300 °C.

1. Introduction

The ternary semiconductor compounds have a wide range of potential applications in device technology due to the presence of three different chemical components that allow, at least in principle, the tailoring of several important physical properties. The physics of these compounds span many areas of fundamental and technological interest. They have been used as light emitting diodes, non-linear optical devices, photochemical cell applications and photovoltaic solar cells [1].

One of these ternary semiconductors which have attracted considerable attention [2] is the compound $CuIn_5S_8$. Thin films and single crystals of $CuIn_5S_8$ have been deposited by various methods, such as sequential process [3], modified Bridgman method [4], single-source organo-metallic chemical vapour deposition [5] and normal freezing method [6]. In literature, some data about the properties of $CuIn_5S_8$ single crystals have been studied [7–9]. However, only few attempts to produce $CuIn_5S_8$ thin films are known [2,3–10]. Among the reported data, it was mentioned that $CuIn_5S_8$ valency has disordered spinel structure (cubic, Fd3 m) on the tetrahedral sites and can be written by the general formula $(Cu^{+1}In^{+3})_t(In_4{}^{+3})_oS_8{}^{-2}$, where the subscripts *t* and *o* indicate tetrahedral and octahedral sites, respectively [11]. The lattice constant is $a = 10.6736$ Å [12]. $CuIn_5S_8$ is an n-type semiconductor with direct transition [5]. The band gap of $CuIn_5S_8$ is near 1.5 eV [13,14] and the temperature dependence of the band gap showed 1.35 and 1.32 eV at 0 K and 300 K, respectively [4–12]. These values are very close to the theoretical values suggested for obtaining a maximum efficiency in solar cell applications [15,16].

To the best of our knowledge, the properties of $CuIn_5S_8$ thin films have never been studied in detail and the effects of thermal treatment have not been reported yet. In this work, we report the synthesis of $CuIn_5S_8$ thin films on glass substrates by thermal deposition technique under particular growth conditions, then, we have studied how structural, optical and electrical characteristics of these films change as a function of annealing in the air in the temperature range 100–300 °C.

2. Experimental details

2.1. Synthesis of $CuIn_5S_8$

Stoichiometric amounts of the elements of 99.999% purity Cu, In, and S were used to prepare the initial ingot of $CuIn_5S_8$. The mixture was sealed in vacuum in a quartz tube. In order to avoid explosions due to sulfur vapour pressure, the quartz tube was heated slowly (20 °C/h). A complete homogenization could be obtained by keeping the melt at 1000 °C for about 48 h. The tube was then cooled at rate 7 °C/h. So, the cracking due to thermal expansion of the melt on solidification was avoided. Crushed powder of this ingot was used as raw material for the thermal evaporation.

* Corresponding author. Tel.: +21697587918.
E-mail address: gm_mounir@yahoo.fr (M. Gannouni).

0925-8388/$ – see front matter © 2011 Elsevier B.V. All rights reserved.
doi:10.1016/j.jallcom.2011.02.047

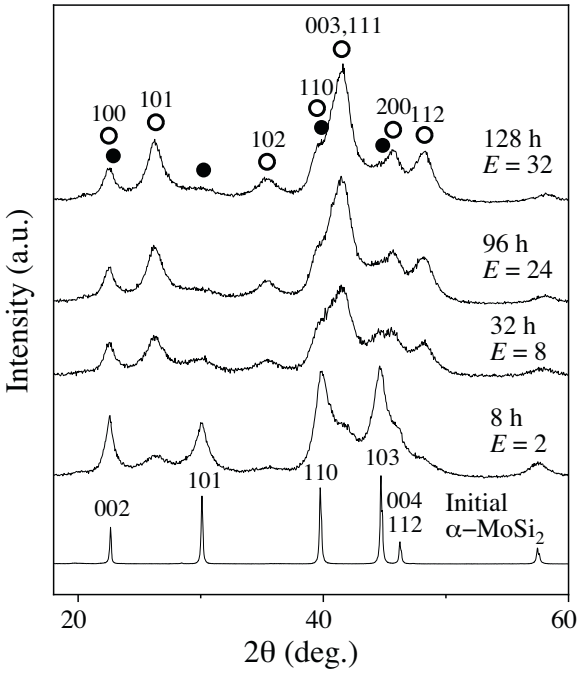

Fig. 1. XRD pattern of $CuIn_5S_8$ powder.

2.2. Film preparation

Evaporated thin films were grown from $CuIn_5S_8$ powder by vacuum evaporation using resistively heated tungsten boats. Thermal evaporation sources were used to be controlled either by the crucible temperature or by the source powder. The pressure during evaporation was maintained at 10^{-6} Torr. Corning 7059 glasses were used as substrates. The film thickness was calculated from the positions of the interference maxima and minima of reflectance spectra using a standard method [17]. The film thickness was found to be ~600 nm. The average deposition rate was around 1 nm s^{-1}. Some of the deposited films were subjected to the post air-annealing procedure in the temperature range 100–300 °C with an increment of 50 °C for 2 h.

2.3. Characterization

The structural properties were determined by the X-ray diffraction technique using CuKα radiation (λ = 1.542 Å). X-ray patterns was carried out to determine the lattice parameter (a), the phases present and the orientation of the synthesized $CuIn_5S_8$ powder and thin films prepared by vacuum deposition method. It is also used for studying the thermal annealing effect on the structure of the as-deposited films. A comparison with JCPDS file cards was done for the establishing the observed peaks. The surface morphology was examined using Philips XL-30 scanning electron microscope (SEM). Optical transmittance and reflectance were measured at normal incidence with an UV–visible-NIR Shimadzu 3100S spectrophotometer in the wavelength range 300–1800 nm at room temperature with the light beam incident on the substrate side with a microglass side as reference. Film resistance was measured between two gold ohmic electrodes previously deposited by thermal evaporation. The type of conductivity of these films was determined by the hot probe method.

3. Results and discussion

3.1. Structural and compositional analysis

3.1.1. Structural of $CuIn_5S_8$ powder

In Fig. 1, XRD pattern of the source powder indicates that it has a single phase of cubic spinel structure and not another phase which exists in the structure. This was verified by JCPDS (Joint Committee on Powder Diffraction Standards) database with card number 24-361 [18]. The main peaks are located at 2θ values of 27.84°, 33.67°, 44.15° and 48.36° with the reflection planes of (3 1 1), (4 0 0), (5 1 1) and (4 4 0) respectively. These reflections in XRD pattern are also in good agreement with the reported values [12]. The Miller indices ($h\,k\,l$), the observed and calculated interplanar spacing (d) and the relative intensities (I/I_0) of the diffraction lines are listed in Table 1. The calculated and observed interplanar spacing are found to be in good agreement with each other. The deduced value of the unit cell parameter for this crystal (a) is found to be 10.667 Å. This value is in good agreement with those reported by several authors [12,19,20]. An examination of the results obtained shows that there are no forbidden reflections ($h\,k\,0$) with $h+k=4n+2$ detected for this compound (check Table 1). The absence of (2 0 0), (4 2 0) and (6 4 0) reflections indicates that there are no "A" site ordering as was observed in analogous chromite spinels [21]. Thus, this crystal can be assigned to the conventional space group Fd3 m [12].

Table 1
X-ray powder diffraction data for $CuIn_5S_8$ crystals (λ_{Cu} = 1.5418 Å).

I/I_0 (%)	Bragg angle 2θ (°)	d_{hkl} (Å) (Calc)	d_{hkl} (Å) (Obs)	($h\,k\,l$)
32	14.514	6.135	6.103	111
29	23.699	3.763	3.754	220
100	27.837	3.203	3.205	311
17	29.082	3.072	3.070	222
51	33.678	2.662	2.661	400
10	36.758	2.442	2.445	331
19	41.515	2.172	2.175	422
44	44.166	2.052	2.051	511
71	48.307	1.882	1.884	440
10	50.677	1.801	1.801	531
12	54.406	1.687	1.686	620
20	56.607	1.628	1.626	533
10	57.288	1.610	1.608	622

3.1.2. Structure of $CuIn_5S_8$ thin films

Fig. 2 shows the results of our XRD measurements for as-deposited and films annealed at 100–300 °C. As seen in the figure, the as-deposited films (Fig. 2a) show amorphous structure in nature. However, under thermal treatment the spectra demonstrate that the films have been always grown with a preferred (3 1 1) orientation according to the angular positions at (2θ = 27.84°) which we have assigned to the cubic $CuIn_5S_8$ spinel phase, this result is in agree with which reported by several authors [5–22]. It is also evident from the figure that two different types of films could be distinguished.

The first one (Fig. 2(b) and (c)), films annealed at 100 and 150 °C showed only one small diffraction peak in the (3 1 1) reflection due to the poor crystallinity of the samples. In the second one, films are annealed at temperatures higher than 200 °C, the films annealed

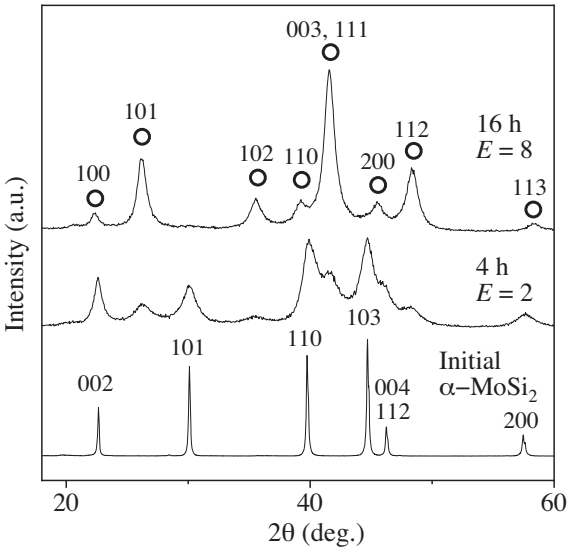

Fig. 2. XRD pattern of as-deposited and thermally annealed $CuIn_5S_8$ thin films.

Table 2
Atomic percentage of constituents of as-deposited and annealed $CuIn_5S_8$ thin films from 100 to 300 °C.

	S_K	In_L	Cu_K	$CuIn_xS_y$
As-deposited	51.12	38.33	10.55	$CuIn_{3.63}S_{4.85}$
100	52.63	37.25	10.13	$CuIn_{3.68}S_{5.2}$
150	52.73	38.24	9.03	$CuIn_{4.23}S_{5.84}$
200	49.17	42.58	8.25	$CuIn_{5.16}S_{5.96}$
250	49.63	42.71	7.66	$CuIn_{5.58}S_{6.48}$
300	49.13	43.17	7.69	$CuIn_{5.61}S_{6.39}$

at 200 °C showed the existence of six peaks associated to the cubic $CuIn_5S_8$ spinel phase (Fig. 2(d)). This number increases when the films were annealed at 250 and 300 °C indicating an enhancement in the crystallinity of the samples. On the other hand, it should be noted, that the preferred orientation of the (3 1 1) peak increases when the annealing temperature increases, which, implies that the surface composition varies with the thermal treatment. Indeed, initially there were many crystallites present in the as-deposited and annealed films below 200 °C that exhibited less intense peaks and when the layers were annealed at a particular temperature above 200 °C, the crystallites are enhanced with an improved crystallinity.

As a result of this study, the annealing treatment has affected both the transition from amorphous phase to polycrystalline phase, the appearance of many peaks and the (3 1 1) preferred orientation intensity of XRD patterns.

3.1.3. Compositional analysis

The chemical composition of $CuIn_5S_8$ thin films annealed at different substrate temperature were carried out using scanning electron microscope SEM, 30XL, Philips make, equipped with energy dispersive analysis of X-rays (EDAX) facilities operated at 30 kV with standardless ZAF quantification. The concentrations of Cu, In and S are shown in Table 2. It can be observed that there is a deficient in the sulfur and copper for all films and an increase in the indium, which becomes excess for the high annealing temperature above 200 °C. The annealing treatment has greatly affected the composition of the films. In this case, it can be seen the deviations of stoichiometry for the as-deposited and annealed films below 200 °C compared to those annealed above 200 °C where they become nearly stoichiometric. The result is in good agreement with the reported by X-ray analysis which confirms the polycrystalline phase with the corresponding temperature.

3.1.4. Morphological properties

The morphological analysis of $CuIn_5S_8$ films was carried out using a Philips XL-30 scanning electron microscope. SEM images have been obtained for samples as-deposited and annealed at different temperatures in order to study their effects on the film surfaces. Fig. 3 shows the micrographs of the as-deposited samples and annealed at 100–300 °C. It is clear from the micrographs that the as-deposited films and annealed films below 200 °C that the surfaces of the films are smooth and there are no isolated particles observed at the surfaces. For the films annealed above 200 °C particles are observed at the surfaces, which infect the entire film surface. Probably, the particles correspond to the indium rich phase for the annealing temperature above 200 °C. For this case, the particles were distributed homogeneously on the surfaces and a difference in number and size with increasing annealing temperatures is observed. So, these results correlate with those obtained by X-ray diffraction and EDX. Indeed, these results show that from the annealing temperature 200 °C the films begin to crystallize and show an Indium rich phase.

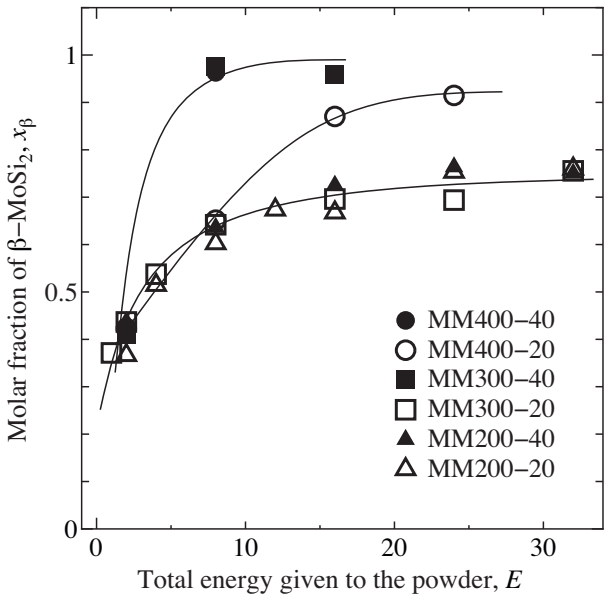

Fig. 3. SEM images of as-deposited and annealed $CuIn_5S_8$ thin films at: 100 °C, 150 °C, 200 °C, 250 °C and 300 °C.

3.2. Optical properties

3.2.1. Optical transmission and reflection spectra.

In order to determine the optical band gap, optical absorption measurements were carried out using

UV–vis spectrophotometer. Fig. 4 shows the transmission and reflection spectra in the wavelength 300–1800 nm at normal incidence for the as-deposited and annealed $CuIn_5S_8$ films. The transmission spectra show that all films exhibit two distinct slopes. The first one ($\lambda > 800$ nm), in which interference fringes are seen, is commonly named the transparency zone or the zone of weak absorption. In the second one ($\lambda < 800$ nm), which is well known as the zone of high absorption, the signal is strongly reduced. An insignificant variation of the rate values of transmission is also observed. A slight increase above 5% in transmittance rate is observed with the increase of annealing temperature. We note also that the films with higher annealing temperature have absorption edges shifted to the low energy side, which indicates small band gaps. However, the reflection spectra show a decrease in the rate values from 55% for the as-deposited to 35% for the annealed films.

3.2.2. Absorption coefficients

By exploiting the different transmission and reflection spectra corresponding to the various annealing temperatures, we were able

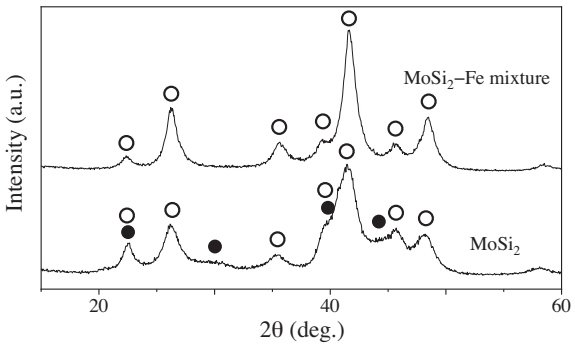

Fig. 4. Optical transmission and reflection spectra of as-deposited and annealed $CuIn_5S_8$ thin films at various temperatures.

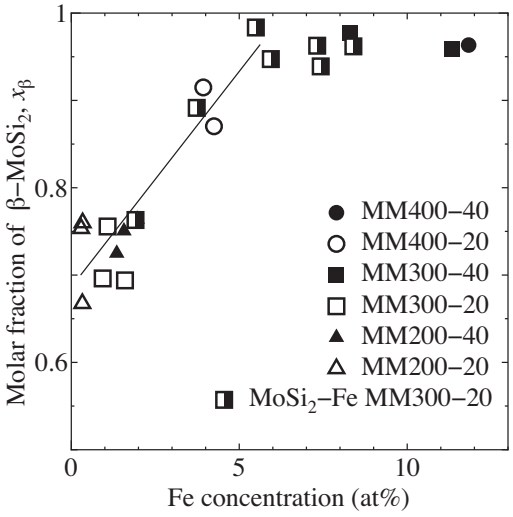

Fig. 5. Absorption spectra of as-deposited and annealed $CuIn_5S_8$ thin films at various temperatures.

to determine the absorption coefficient $\alpha(h\nu)$, using the following relation [23,24]:

$$\alpha = \frac{1}{d}\ln\left[\frac{(1-R)^2}{T}\right] \quad (1)$$

where d is the film thickness, R and T are the reflection and transmission coefficients respectively. Fig. 5 shows the absorption coefficients versus the photon energy for the as-deposited and annealed films at various temperatures. It is clear from the figure that the absorption coefficient of the samples exceeds $10^4\ cm^{-1}$ and sharply increases with increasing photon energy in the region of 1.45–2.1 eV. This result is very important because we know that the spectral dependence of the absorption coefficient affects the solar conversion efficiency [25].

3.2.3. Energy gaps

To obtain detailed information about the energy ban gap of the material, the α–E dependences for the as-deposited and annealed films in the sharp absorption region where α can be represented by Eq. (2) [26]:

$$(\alpha E) = B(E - E_g)^p \quad (2)$$

In this equation, B is a constant that depends on the transition probability, h is the Planck constant and p is an index that characterizes the optical absorption process and it is theoretically equal to 2, 1/2, 3 or 3/2 for indirect allowed, direct allowed, indirect forbidden and direct forbidden transitions. The best plot that covers widest range of data – in accordance with Eq. (2) – was obtained for the $(\alpha E)^2$–E dependence. This plot is illustrated in Fig. 6. The E-axis interception in this figure reflects the direct allowed transitions in $CuIn_5S_8$ thin films. As can be seen in the figure, there is a shift in the band gap energy towards lower energies during transformation from the amorphous to polycrystalline phase that takes place at higher annealing temperature $T > 200\,^{\circ}C$. The values of E_g^d obtained are shown in Table 3 as a function of thermal annealing treatment and in this table we can observe that direct band gap energy decreases from 1.83 eV for the as-deposited films to 1.43 eV for the films annealed at 300 °C.

Up to our knowledge, the annealing temperature dependence of the band gap for the $CuIn_5S_8$ thin film is not yet studied. In polycrystalline semiconductors, several possible reasons that contribute to a decrease in band gaps have been postulated [27,28]. In the present study, the decrease of optical band gap could be attributed to the stoichiometric deviations in the films, which give rise to the formation of localized states in the band gap region. These states might be induced in the band gap because of the structural disorder due to the sulfur deficiency, or it results from excess indium, which creates localized states in the band gap and consequently decreases the optical energy gap.

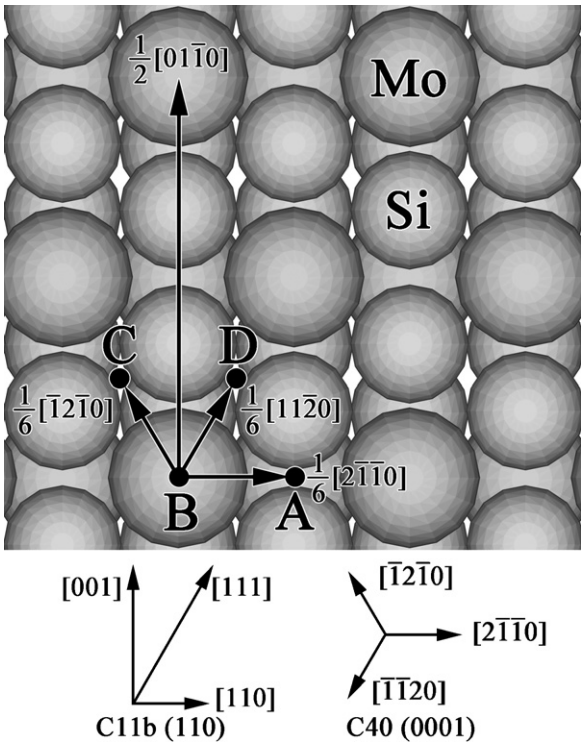

Fig. 6. Plots of $(\alpha h\nu)^2$ versus $(h\nu)$ for the $CuIn_5S_8$ thin films at various annealing temperatures.

3.3. Electrical properties

Film resistance was measured between two gold ohmic electrodes previously deposited by thermal evaporation. The type of conductivity of these films was determined by the hot probe method.

It was found that initially the layers are highly compensated because of their relatively high resistivities (>200 MΩ) and there is no specific type of conductivity that was observed. The study of the annealing at free air allowed the transformation of the highly compensated state layer in a semiconductive state (∼10 kΩ), which exhibited n-type conductivity for annealing temperature from 300 °C. This change could be interpreted in terms of phase evolution. The thermal treatment is an efficient way to stabilize the n-type $CuIn_5S_8$ thin films.

Table 3
Variation of direct optical band gap of $CuIn_5S_8$ thin films with different annealing temperatures.

Annealing temperature (°C)	Direct optical band gap (eV)
As-deposited	1.83
100	1.63
150	1.56
200	1.54
250	1.49
300	1.43

4. Conclusions

The obtained $CuIn_5S_8$ crystals have a single phase of cubic spinel structure related to the conventional space group Fd3 m structure. The value of the unit cell parameter (a) for this crystal is found to be 10.667 Å.

Thin films of $CuIn_5S_8$ were successfully deposited onto glass substrates by thermal evaporation and annealed in air from 100 °C to 300 °C for 2 h. Post-depositional annealing effects on structural, optical and electrical properties of thermal evaporated $CuIn_5S_8$ thin films were studied. The most important effects are:

- Transition from the amorphous to the polycrystalline structure, which, depending on the thermal annealing treatment, occurs at 200 °C. The annealing causes better crystallization and lead to the appearance of more intensive peaks.
- Deviations from stoichiometry for the as-deposited and annealed films below 200 °C, which thereafter become nearly stoichiometric under annealing temperature above 200 °C.
- Displacement of the absorption edge to lower energies with increasing the annealing temperature causing the decrease of the band gap energies from 1.83 eV to 1.43 eV for the as-deposited and annealed films at 300 °C, respectively. This change may be related to the compositional change by post-heat treatment.
- Conversion from the intrinsic to n-type conductivity below and above 300 °C, respectively.

Finally, these characteristics reported in this work make this material attractive as an absorber material in solar cells applications.

References

[1] A.F. Qasrawi, J. Alloys Compd. 455 (2008) 295–297.
[2] I. Konovalov, O. Tober, M. Winkler, K. Otte, Sol. Energy Mater. Sol. Cells 67 (2001) 49.
[3] V. Liudmila, I. Makhova, R. Konovalov, Szargan, Phys. Stat. Sol. 201 (2004) 308–311.
[4] A.F. Qasrawi, N.M. Gasanly, Cryst. Res. Technol. 38 (2003) 1063–1070.
[5] Ryôki Nomura, Yasuharu Seki, Haruo Matsuda, Thin Solid Films 209 (1992) 145–147.
[6] S. Kitamura, S. Endo, T. Irie, Thin Solid Films 209 (1992) 145–147.
[7] N.S. Orlova, I.V. Bodnar, E.A. Kudritskaya, Cryst. Res. Technol. 33 (1998) 37.
[8] S. Endo, S. Kitamura, T. Irie, Nuovo Cimento 2D (1983) 1875.
[9] S. Takaeuchi, S. Endo, T. Irie, Phys. Chem. Solids 46 (1985) 887.
[10] S. Kobayashi, N. Tsuboi, T. Sega, K. Oishi, F. Kaneko, Jpn. J. Appl. Phys. 42 (2003) 5485.
[11] N. Greenwood, Ionic Crystals—Lattice Defects and Nonstoichiometry, Butterworths, London, 1968.
[12] A.F. Qasrawi, N.M. Gasanly, Cryst. Res. Technol. 36 (2001) 12.
[13] A. Usujima, S. Takeuchi, S. Endo, T. Irie, Jpn. J. Appl. Phys. 20 (1981) L505.
[14] R.S. Becker, T. Zheng, J. Elton, J. Electrochem. Soc. 132 (1985) 1824.
[15] G. Dagan, S. Endo, G. Hodes, G. Sawatzky, D. Cahen, Sol. Energy Mater. 11 (1984) 57 [7] H.
[16] Minoura, Y. Ueno, H. Kaigawa, T. Sugiura, J. Electrochem. Soc. 136 (1989) 1392.
[17] O.S. Heavens, Optical Properties of thin Solid Films, Butterworths, London, 1950.
[18] Robbins, Miksovsky, Mater. Res. Bull. 6 (1971) 359.
[19] L. Gastaldi, L. Scarmuzza, Acta Cryst. B35 (1979) 2283.
[20] C. Paorici, L. Zanotti, N. Romeo, G. Sberveglieri, L. Tarricone, Mater. Res. Bull. 12 (1977) 1207.
[21] H. Hirotaka, S. Chirba, J. Phys. Soc. Jpn. 27 (1969) 505.
[22] L. Makhova, R. Szargan, I. Konovalov, Thin Solid Films 472 (2005) 157–163.
[23] D.E. Milovzorov, A.M. Ali, T. Inokuma, Y. Kurata, T. Suzuki, S. Hasegawa, Thin Solid Films 382 (2001) 47.
[24] T.M. Wang, S.K. Zheng, W.C. Hao, C. Wang, Surf. Coat. Technol. 155 (2002) 141.
[25] V.V. Kindyak, V.F. Gremenok, I.V. Bodnar, Y.V. Rud, G.A. Madvedkin, Thin Solid Films 250 (1994) 33–36.
[26] J.I. Pankove, Optical Processes in Semiconductors, Prentice-Hall, New Jersey, 1971, p. 93.
[27] J Tauc, A.J. Menth, Non-Cryst. Solids 8 (1972) 569.
[28] N.F. Mott, E.A. Davis, Electronic processes in non-crystalline materials, Oxford University Press, London, 1977, p. 340.